ACS OMEGA

Article

http://pubs.acs.org/journal/acsodf

A Multifunctional Protein Coating for Self-Assembled Porous Nanostructured Electrodes

Xuewei Fu,[†] Yu Wang,*[,†] Wei-Hong Zhong,*[,†] and Guozhong Cao[‡]

[†]School of Mechanical and Materials Engineering, Washington State University, Pullman, Washington 99164, United States

[‡]Department of Materials and Engineering, University of Washington, Seattle, Washington 98195-2120, United States

Supporting Information

ABSTRACT: Creation of three-dimensional (3D) porous nanostructured electrodes with controlled conductive pathways for both ions and electrons is becoming an increasingly important strategy and is particularly of great interest for the development of high-performance energy storage devices. In this article, we report a facile and environmentally friendly self-assembly approach to fabricating advanced 3D nanostructured electrodes. The self-assembly is simply realized via formation of a multifunctional protein coating on the surface of electrode nanoparticles by using a denatured soy protein derived from the abundantly prevalent soybean plant. It is found that the denatured protein coating plays three roles simultaneously: as a surfactant for the dispersion of electrode nanoparticles, an ion-conductive coating for the active materials, and a binder for the final electrode. More importantly, it is interestingly found that being a unique surfactant, the surface protein coating enables the self-assembly behavior of the electrode nanoparticles during the evaporation of aqueous dispersion, which finally results in 3D porous nanostructured electrodes. In comparison with the most classic binder, poly(vinylidene fluoride), the advantages of the 3D nanostructured electrode in terms of electrochemical properties (capacity and rate capability) are demonstrated. This study provides an environmentally friendly and cost-effective self-assembly strategy for fabrication of advanced nanostructured electrodes using electrode nanoparticles as the building block.

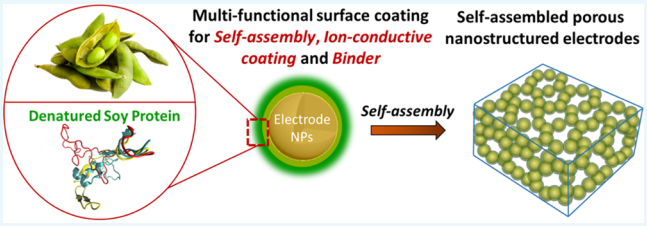

INTRODUCTION

Nanostructured electrodes enabling fast charge transfer and electrochemical reactions play a vital role in achieving both high energy and power densities for energy storage devices (ESDs).[1−4] In particular, developing advanced nanostructured electrodes for lithium ion batteries is believed to be one of the most effective solutions for satisfying the increasing demand for high energy and power densities for ESDs. This is considered as key to the success of electric vehicles.[5,6] As a result, strategies on the fabrication of nanostructured electrodes have attracted great interest over the past decades.[7−10] In general, the strategies reported for ESDs (e.g., lithium ion batteries) can be classified into several types as follows. The first one, also the most common, is based on the fabrication of active nanoparticles via nanofabrication techniques, such as the hydrothermal process[11,12] and aerogel synthesis.[13,14] A variety of nanoparticles, such as nanospheres,[15,16] nanorods,[17,18] and nanosheets,[19,20] were presented by using this strategy to produce nanostructured electrodes. The procedures for electrode preparation usually follow the conventional methods for designing a porous electrode. The second strategy consists of fabricating nanofabrics as electrodes.[21−23] For this strategy, the active materials are either made into nanofibers or deposited on a nanofabric template. The nanofabrics provide a good combination of porous structures for ion conduction and connect conductive networks for electron conduction. A template-based method can be referred to as the third strategy, which includes soft templating,[24,25] hard templating,[26,27] and so forth. On the basis of this strategy, fabrication of various nanostructured active materials, such as TiO_2, SnO_2, $LiMnO_2$, and so on,[8,9,28,29] has been reported. For the template-based method, one can precisely control the porous structures and the morphology of the nanostructured electrodes. The fourth well-known strategy is deposition. Various deposition techniques, such as electrodeposition,[30,31] chemical vapor deposition,[32,33] and chemical bath deposition,[34,35] are widely employed to grow nanostructured electrodes directly on the current collectors.

Although these strategies have been widely used and have achieved great success, developing more cost-effective strategies for fabrication of three-dimensional (3D) nanostructured electrodes is becoming more critical for practical applications. Because almost all of the electrode materials can be converted into nanoparticles, it would be extremely helpful if one could introduce self-assembly behavior to these electrode nanoparticles simply by surface treatment. In fact, polymer binders, usually necessary in the fabrication of electrodes, might have this potential provided they are rationally designed. However, traditional binders are merely binder materials, which fail to represent functions in addition to binding active materials. These binders include poly(vinylidene fluoride) (PVDF),[36,37]

Received: March 10, 2017
Accepted: April 17, 2017
Published: April 27, 2017

DOI: 10.1021/acsomega.7b00289
ACS Omega 2017, 2, 1679−1686

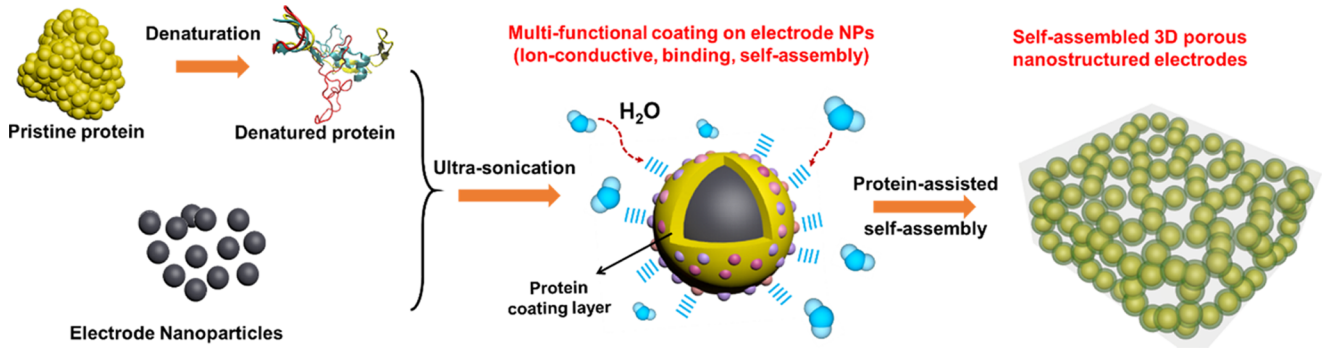

Figure 1. Schematic of the fabrication strategy for the nanostructured porous electrodes via a multifunctional surface coating. The SP was first denatured to unfold the functional groups of amino acids. Then, the denatured proteins act as a multifunctional surfactant, which gives rise to the self-assembly of electrode nanoparticles and finally a self-assembled porous electrode.

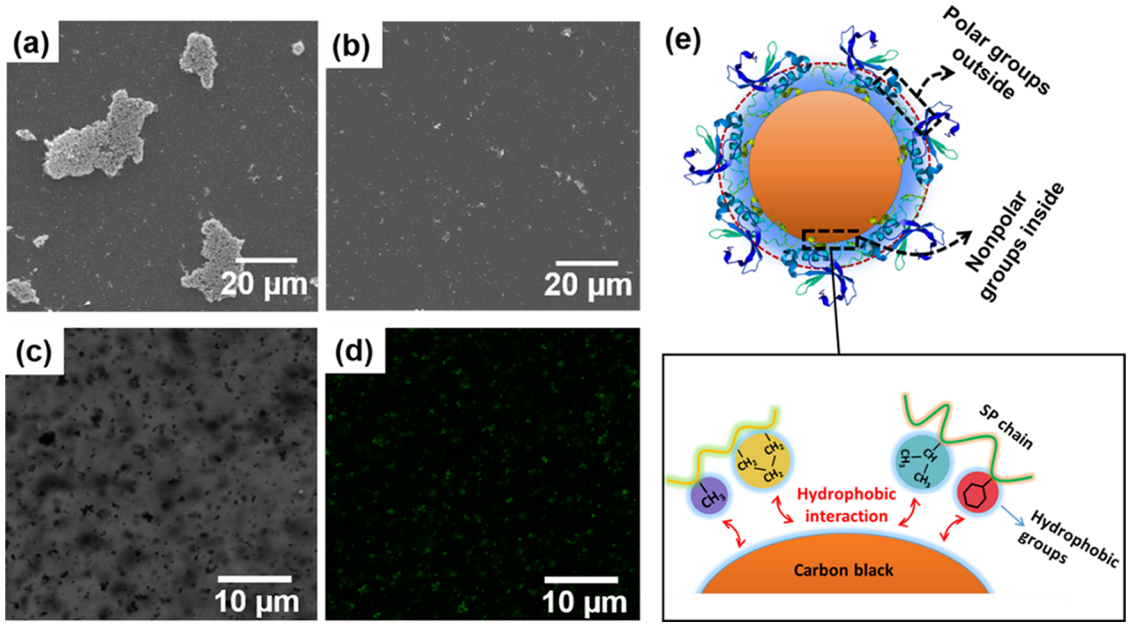

Figure 2. Surface coating of electrode nanoparticles by denatured protein. (a)−(b) scanning electron microscopy (SEM) images of the dispersed CB particles without and with d-SP surface treatment. Confocal microscopy images of d-SP treated CB (SP@CB) dispersed in PEO solution: (c) transmission mode without fluorescent light, (d) fluorescent mode with green color from d-SP. (e) Illustration of the interaction between d-SP and CB.

carboxymethyl cellulose (CMC),[38,39] carboxymethyl chitosan,[40,41] polyacrylic acid (PAA),[42,43] gelatin,[44,45] and so on. To achieve more functions from the binder, which is critical for better electrochemical performance, conductive binder materials have recently been of great interest. Specifically, conducting polymers, such as poly(3,4 ethylenedioxythiophene) (PEDOT),[46,47] poly(ethylene oxide) (PEO),[48] and polypyrrole (PPy),[49,50] have been reported as advanced binder materials for high-capacity electrodes, such as sulfur and silicon. The conductive binders actually play two roles simultaneously: binding the active materials and transporting ions/electrons inside the electrodes. It is believed that conductive binders provide an effective solution to improving the electrochemical performance of ESDs. However, these reported conductive binders are usually unable to introduce self-assembly behavior to the electrode nanoparticles, which is an attractive strategy for controlling the porous structures, as are the ion/electron conductive pathways for electrodes.

To address the limitations of conventional conductive binders, we report a novel strategy using denatured soy protein (d-SP) to form a multifunctional surface coating on electrode nanoparticles. Our previous studies have demonstrated that d-SP is an effective surfactant for facilitating dispersion of graphitic materials, such as carbon nanotubes[51,52] and graphite nanoplatelets[53] in water and even in a polymer matrix. More importantly, our recent work revealed that d-SP also presents great potential in being an advanced ion conductor for lithium ions.[54] On the basis of these significant findings, herein, we further demonstrate that d-SP can be employed as a "green" multifunctional binder material, which integrates the multiple roles of ion conductor, surfactant, and binder, in addition to the self-assembly of electrode particles. As a result, a self-assembled 3D porous nanostructured electrode is successfully fabricated, and its contribution to the electrochemical performance of the electrode is confirmed by this study.

RESULTS AND DISCUSSION

Figure 1 illustrates the procedure of fabricating a 3D porous nanostructured electrode via a multifunctional protein surface coating. As shown, native soy proteins (SPs) are big powders,

DOI: 10.1021/acsomega.7b00289
ACS Omega 2017, 2, 1679−1686

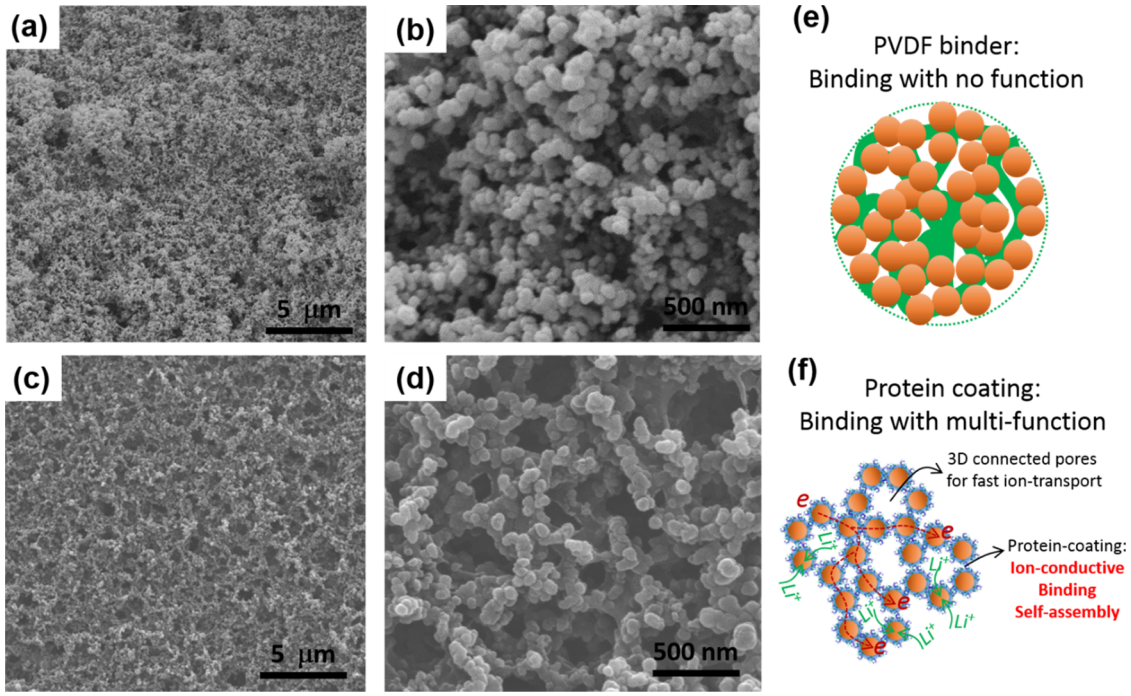

Figure 3. Three-dimensional porous nanostructured electrodes based on the multifunctional protein coating as compared with those based on the traditional PVDF binder. SEM images of PVDF@CB (a, b) and SP@CB (c, d). (e, f) Illustration of the microstructure of PVDF@CB and SP@CB.

bonded by very strong interchain interactions, including hydrogen bonding, disulfide bonding, and hydrophobic interactions, which enclose a large amount of functional groups.[55] Denaturation of SP breaks down the quaternary, tertiary, and even secondary structures of the protein and discloses the polar/nonpolar functional groups of the polypeptide.[56] The particle size of SP is dramatically reduced after denaturation from ca. 50 μm to ca. 30 nm[57] to form a yellowish solution. The d-SP acts as a surfactant, and the nonpolar groups of d-SP (aromatic residues in particular) can strongly interact with the surface of carbon nanomaterials through the $\pi-\pi$ stacking interaction;[51,57] therefore, the dispersion of carbon black (CB) in aqueous solvent is significantly improved due to the polar groups of d-SP. During evaporation of the solvents, the protein-coated CB nanoparticles self-assemble into a porous configuration with the aid of the protein. Finally, the protein coating acts as a binder as well as an ion-conductive coating for the final electrode.

To confirm the surface coating of d-SP on the CB surface, we performed studies on the dispersion, morphology, and fluorescent properties of the d-SP treated CB. As shown in Figure 2a,b, the agglomeration of CB particles is greatly reduced in d-SP solution as compared to that without d-SP surface treatment (also see the optical microscopy images in Figure S1, Supporting Information). The study indicates that d-SP can act as an effective surfactant for the electrode nanoparticles of CB. To further investigate that d-SP is coated onto the surface of CB, we performed a fluorescence study to obtain confocal images, which reveals the location of the protein by absorption of fluorescent light. The results shown in Figure 2c,d suggest that the location of green fluorescence from SP (see Figure 2d) is well in accordance with the location of CB, as shown in Figure 2c, which were taken from the same place as that of the sample (also see fluorescence property of d-SP as the control sample in Figure S2). All of the above results indicate that the d-SP, acting as a unique surfactant, was successfully coated onto the CB nanoparticles. The possible mechanism for the interactions between CB and d-SP is illustrated in Figure 2e. It is believed that the hydrophobic nature of the CB surface can strongly interact with the nonpolar groups of d-SP, such as aromatic groups, methyl groups, and so on, as shown in the inset of Figure 2e. At the same time, the polar hydrophilic groups of d-SP are exposed to the aqueous solvent.

It was interestingly found that there is a big difference in the microstructures of the two samples: PVDF@CB and SP@CB. For PVDF@CB, although there are lots of pores, as shown in Figure 3a,b, the porous structure is irregular and most of the pores are found only on the surface. In contrast, for the SP@CB electrode, the porous structures are more uniform and more connected in 3D space, as shown by Figure 3c,d. As proteins have been reported as effective agents for introducing self-assembly to nanoparticles,[58,59] it is believed that the porous nanostructure of SP@CB is related to a unique self-assembly behavior of the d-SP-treated CB during the evaporation of the solvent. Owing to the fact that SP contains some residual lipid, which may also act as a type of surfactant, we further confirm the role of the protein as a surfactant by performing a parallel study on another type of protein, gelatin. In contrast to SP, gelatin is a pure protein but possesses a similar amino acid profile as SP. As such, we also fabricated the electrodes using gelatin as the surfactant. With the same ratios and preparation conditions, a very similar porous nanostructure was obtained (see Figure S4 for SEM images), which further confirms that the protein is responsible for the self-assembly behavior of the electrode nanoparticles.

Moreover, it is also believed that the drying process is another critical factor controlling the formation and morphology of the nanostructured materials, that is, the kinetics of the self-assembly process. To investigate this factor, the samples were dried at different temperatures. At 25 °C, it was found that the high percentage of acetic acid (80 wt %) gives rise to a very

DOI: 10.1021/acsomega.7b00289
ACS Omega 2017, 2, 1679−1686

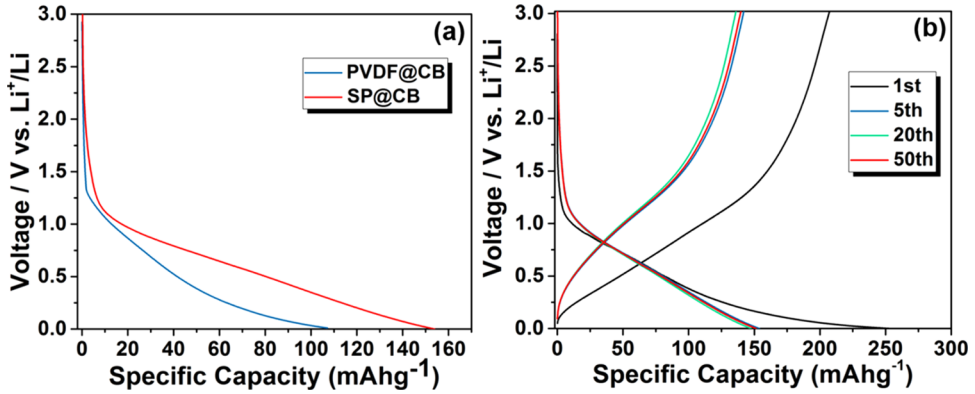

Figure 4. Electrochemical performance of the porous SP@CB electrode as compared with that of PVDF@CB at a low current density of 60 mA g^{-1}. (a) Galvanostatic discharge profile between 3 and 0 V for the second cycle. (b) Galvanostatic charge−discharge profiles of the SP@CB electrode at the 1st, 5th, 20th, and 50th cycle.

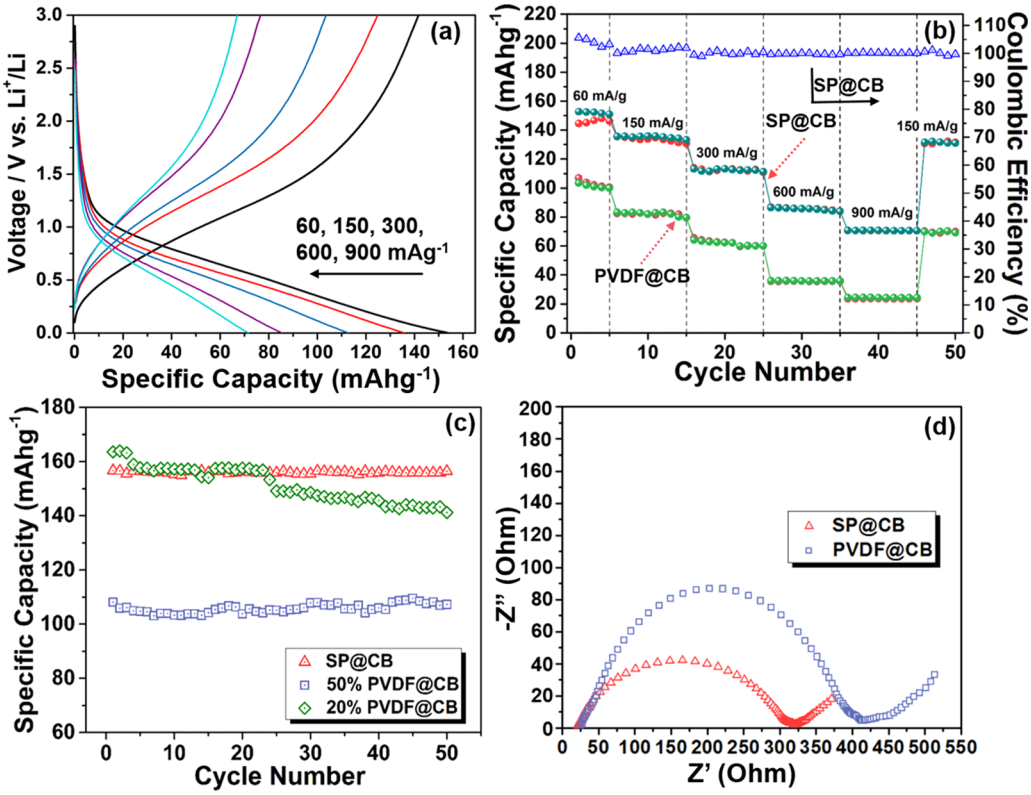

Figure 5. Rate capability and cycle performance of the porous SP@CB electrode as compared with those of PVDF@CB. (a) Galvanostatic charge−discharge profiles of the SP@CB electrode at various current densities. (b) Rate capability of the SP@CB electrode at varying current rates as compared with that of PVDF@CB. (c) Cycling performance comparison at a current density of 60 mA g^{-1}. (d) Nyquist plots of fresh half-cells based on SP@CB and PVDF@CB electrodes at a frequency range of 0.01−1 MHz.

fast drying speed, which results in a homogeneous solid electrode sample in only ca. 15 min, as shown in Figure S5a. However, when increasing the temperature to 50 °C to speed up the drying process, a distinctive phase separation occurred, as shown in Figure S5b, possibly due to the different boiling points of the two solvents (H_2O and acetic acid). Therefore, to obtain a homogeneous electrode, the appropriate drying speed is very important.

As mentioned previously, the 3D connected porous nanostructured electrode can greatly benefit the charge transfer and electrochemical reaction, which are critical for the electrochemical performances of the electrodes. Figure 3e,f illustrate the difference in microstructure for the two samples (see more SEM images in Figure S3). Specifically, the PVDF@CB sample shows an uncontrolled porous structure, which results from a random accumulation of the CB nanoparticles during evaporation. However, the SP@CB sample exhibits a more controlled, continuous, and uniform porous nanostructure, which is related to the protein-directed self-assembly of the CB nanoparticles. In addition to the contribution to microstructures of the electrode, the protein coating also plays two other roles: as a binder for the electrode and an ion-conductive coating of the electrode nanoparticles, which has been revealed in our recent studies on using the protein−ion complex as an advanced ion conductor.[54]

DOI: 10.1021/acsomega.7b00289
ACS Omega 2017, 2, 1679−1686

To demonstrate the advantages of the self-assembled, porous, nanostructured electrode, the electrochemical performance of the CB-based electrodes was characterized at room temperature. Figure 4a compares the discharge curves of SP@CB and PVDF@CB at the same current density of 60 mA g^{-1}. It can be found that the specific discharge capacity of SP@CB (154 mA h g^{-1}) is greatly higher than that of PVDF@CB (107 mA h g^{-1}). At the same time, a very high initial discharge capacity (~262 mA h g^{-1} at 60 mA g^{-1}) was achieved by SP@CB, and then the discharge capacity gradually stabilized around 150 mA h g^{-1} at a current density of 60 mA g^{-1} (Figure 4b). The initial capacity loss might be related to the formation of the solid-electrolyte interphase (SEI).[60] The notable capacity loss related to SEI formation also indicates that the SP@CB sample possesses a high surface area for electrochemical reactions, which is consistent with the 3D porous structures, as shown by the SEM images in Figure 3c,d.

Another significant contribution of the 3D porous nanostructures to electrochemical performance is the improvement in rate capability. Therefore, the SP@CB and PVDF@CB electrodes were tested at various current densities of 60, 150, 300, 600, and 900 mA g^{-1}. As shown in Figure 5a, for porous SP@CB, the charge−discharge profiles at different current densities are very similar, which indicates that the lithiation/delithiation process behaves reversibly and stably at different current densities. Figure 5b compares the rate capability between SP@CB and PVDF@CB. It is found that the discharge capacities of both SP@CB and PVDF@CB are very stable at a certain current density. However, the capacity of PVDF@CB decayed dramatically when the current density increased from 60 to 900 mA g^{-1}. The capacity retention is only about 29%. In contrast, as for SP@CB, the capacity retention is around 50% when the current density increased from 60 to 900 mA g^{-1}. Moreover, the SP@CB electrode can recover a specific capacity of 130 mA h g^{-1} at a current density of 150 mA g^{-1}, indicating a high capacity retention rate of 96% after the C-rate testing. However, for PVDF@CB, the capacity retention rate is about 90% after the same C-rate testing, as shown in Figure 5b.

In addition to the excellent rate capability, the porous SP@CB also shows good cycle stability. As displayed in Figure 5c, after 50 cycles at a current density of 60 mA g^{-1}, the capacity of SP@CB is almost the same as the initial capacity of 154 mA h g^{-1} and no evident capacity loss can be observed. Moreover, the capacity of SP@CB is much more stable than that of PVDF@CB. For the control sample containing PVDF, it is noted that the loading of active material (50 wt %) is greatly lower than the classic loading for commercial electrodes (ca. 80 wt %). The extra PVDF may form a thick coating surface on the active materials and deteriorate the electrochemical performance. Therefore, another control sample with 20 wt % loading of PVDF was prepared, and the comparison of the cycling performance is shown in Figure 5c. At the same current rate of 60 mA g^{-1}, this control electrode delivers a discharge capacity of 161 mA h g^{-1}, which is slightly greater than that of the SP@CB electrode (154 mA h g^{-1}). However, as seen in Figure 5c, this control electrode shows a faster capacity decay as compared with that of the SP@CB electrode. In particular, the capacity faded even faster after the 23rd cycle, and the capacity is much lower than that of the SP@CB electrode afterward. The poor cycling performance of this control sample is possibly due to unstable structures or poor dispersion of the electrode nanoparticles. Therefore, the SP@CB electrode shows advantages in terms of specific capacity and cycle stability as compared with those of the PVDF ones.

At the same time, the Nyquist plots, as shown in Figure 5d for SP@CB and PVDF@CB electrodes, further confirm that porous SP@CB possesses a much lower charge transfer resistance because the diameter of the semicircle reflects the charge transfer resistance of the electrode.[40,46] These good electrochemical performances of the SP@CB electrode should be attributed to the following factors. First, the protein surface coating plays the role of an advanced binder, which gives rise to good structure and cycle stability. Second, the protein surface coating is also ion conductive and can significantly facilitate the charge transfer and ion conductions of the electrode particles, which can be revealed by the low resistance for charge transfer and high specific capacity. Third, the self-assembled porous structure is one of the keys for good rate capability.

To investigate the possible contribution of the d-SP to lithium ion storage, a d-SP/CB composite with 80 wt % loading of d-SP was prepared and tested in a half-cell. In this case, d-SP is assumed to be an active material. It was found that the capacity of the entire electrode, including d-SP and CB, is only 16 mA h g^{-1}. As shown in Figure S7a, if d-SP is not viewed as an electrode material, the specific capacity for CB is about 82 mA h g^{-1}, which is still far below that of the porous nanostructured SP@CB electrode (154 mA h g^{-1}). In addition, the Nyquist plot of the SP/CB composite sample (Figure S7b) shows one well-defined semicircle in the high-frequency region with a much larger charge transfer resistance as compared with that of the SP@CB nanostructured electrode. These results indicate that the d-SP itself has negligible or even no capacity for lithium ion storage. Therefore, it is further confirmed that the enhancement of electrochemical properties of the above porous SP@CB electrode is owing to the self-assembled 3D porous nanostructure and the ion-conductive surface coating.

CONCLUSIONS

In summary, we have demonstrated a multifunctional protein surface coating of electrode nanoparticles to fabricate 3D porous nanostructured electrodes via self-assembly. The protein surface coating can play three roles simultaneously: as a surfactant of the electrode nanoparticles that drives self-assembly during evaporation, an ionic conductive coating that facilitates the ion-transfer between electrolyte and electrode, and, finally, a stable binder that maintains the structures for stable cycling. Benefiting from its multifunctionalities, the capacity, cycle stability, and rate capability of the resultant self-assembled porous electrode are significantly improved as compared with those of traditional electrodes. This study provides a cost-effective and important strategy for fabrication of porous nanostructured electrodes via the self-assembly of electrode nanoparticles.

EXPERIMENTAL SECTION

Sample Preparation. SP isolate powders (Archer Daniels Midland Co.) were denatured in a mixture of solvent (80 wt % acetic acid, 20 wt % H_2O) with an ambient pH value of ca. 1.8 at a 3 wt % SP concentration. Specifically, the mixed solvent was first preheated to 95 °C prior to the addition of SP. SP powders were then slowly and slightly added into the solvent with vigorous stirring. The dispersion containing SP was stirred at 95 °C for 1 h to form a yellowish solution. To fabricate the electrodes, nanoparticles of CB (SuperC45; MTI) are

DOI: 10.1021/acsomega.7b00289
ACS Omega 2017, 2, 1679−1686

employed as an example of electrode nanoparticles. Typically, the denatured SP (d-SP) solution was first cooled to room temperature. The electrode nanoparticles were dispersed into 5 mL of the solution of d-SP with the aid of an ultrasonifier (Branson 250) with an amplitude of 15% for 3 min in an ice bath. The weight ratio between SP and CB is 1:1. Finally, the homogeneous dispersion was casted by a film applicator controlling the thickness of the solution constant onto copper foil and evaporated at room temperature, which drives the self-assembly of the electrode nanoparticles. The solid electrode sample was further dried at 60 °C in a vacuum oven for 12 h and then transferred into a glovebox. The reference sample was prepared by mixing the same CB with PVDF binder solution in NMP (M_w = 530 000 g/mol, Sigma-Aldrich), wherein PVDF powders were first dissolved in NMP (VWR) at a concentration of 5 wt %. The weight ratio between the CB and PVDF binder is the same as that for the SP system. This control sample was also dried under the same conditions, as described above. The weight of active material of each electrode was determined at 0.6−0.7 mg/cm^2. The thicknesses of all of the samples were measured by using a digital micrometer. The thickness of SP@CB electrodes is 13 ± 3 μm and it is 17 ± 2 μm for the PVDF@CB electrodes. For confirming the role of the protein that directs the self-assembly, a parallel experiment was also performed on gelatin protein (type A, from porcine skin, Sigma-Aldrich). The gelatin solution was prepared by dissolving the gelatin powders in the same solvent (80 wt % acetic acid, 20 wt % H_2O) at a concentration of 3 wt %. To prepare the gelatin-containing electrodes, the procedures are exactly the same as those for the preparation of SP@CB electrodes. The density of the d-SP was measured as follows. The 3 wt % d-SP solution was first casted onto aluminum foil to be dried at room temperature to obtain solid d-SP films. The d-SP films were further dried in a vacuum oven at 60 °C for 12 h to remove all residual solvents. The weight of the dried d-SP films was then measured. To evaluate the volume, the d-SP films were immersed in NMP solvent in a cylinder, and the volume change of the solvent was recorded, which referred to the volume of the d-SP. Three measurements have been performed to obtain the average density. The density can then be calculated based on the obtained weight and volume, and it was determined to be ca. 1.32 g/cm^3.

Structural Characterization. The morphology of all of the samples was characterized by SEM (Quanta 200F) and optical microscopy (Olympus BX51). For the optical microscopy observation, a very small amount of suspension sample was directly casted on a glass substrate and was covered by a coverslip to observe the dispersion of the CB particles. Prior to the optical microscopy observation, the suspension samples were treated by sonifier for 3 min to disperse CB particles in the solvents. For confocal microscopy characterization, the suspension samples were dispersed in PEO (M_w = 100 000 g/mol, Sigma-Aldrich) solution for stable particle detection. Confocal images were acquired using a ZEISS confocal microscope. The 488 nm line from an argon laser was used for excitation, and fluorescence emission was detected using a 510 nm band-pass filter.

Cell Assembly and Electrochemical Characterization. Half cells with lithium metal as the counter electrode were assembled into a coin cell in an argon-filled glovebox. A commercial separator (Celgard, trilayer PP/PE/PP) was soaked in liquid electrolyte (1 M $LiPF_6$ in EC/DMC, volume ratio: 1:1, Sigma-Aldrich). Prior to employing a separator, one droplet of liquid electrolyte was dropped onto the surface of the prepared CB electrode to wet the surface. The electrochemical performance of the half-cells was examined by cycling the cells between 3 and 0 V by using a battery analyzer (BST8-MA; MTI) at room temperature. Electrochemical impedance spectroscopy was used to measure the impedance of the cells via an electrochemical workstation (CHI660E) over a frequency range of 0.01−10^6 Hz.

■ ASSOCIATED CONTENT

Supporting Information

The Supporting Information is available free of charge on the ACS Publications website at DOI: 10.1021/acsomega.7b00289.

Details of the experimental methods, morphology characterization, and electrochemical property measurements (PDF)

■ AUTHOR INFORMATION

Corresponding Authors

*E-mail: yu.wang3@wsu.edu (Y.W.).

*E-mail: katie_zhong@wsu.edu (W.-H.Z.).

ORCID

Wei-Hong Zhong: 0000-0002-1232-4147

Guozhong Cao: 0000-0003-1498-4517

Notes

The authors declare no competing financial interest.

■ ACKNOWLEDGMENTS

This work was supported by USDA NIFA 2015-67021-22911 and NSF CMMI 1463616. The authors also gratefully acknowledge the support for characterizations from the Franceschi Microscopy & Imaging Center and the Composite Materials and Engineering Center at Washington State University.

■ REFERENCES

(1) Mukherjee, R.; Krishnan, R.; Lu, T. M.; Koratkar, N. Nanostructured Electrodes for High-Power Lithium Ion Batteries. *Nano Energy* **2012**, *1*, 518−533.

(2) Liu, D.; Cao, G. Engineering Nanostructured Electrodes and Fabrication of Film Electrodes for Efficient Lithium Ion Intercalation. *Energy Environ. Sci.* **2010**, *3*, 1218.

(3) Lu, Q.; Chen, J. G.; Xiao, J. Q. Nanostructured Electrodes for High-Performance Pseudocapacitors. *Angew. Chem., Int. Ed.* **2013**, *52*, 1882−1889.

(4) Song, M. K.; Park, S.; Alamgir, F. M.; Cho, J.; Liu, M. Nanostructured Electrodes for Lithium-Ion and Lithium-Air Batteries: The Latest Developments, Challenges, and Perspectives. *Mater. Sci. Eng., R* **2011**, *72*, 203−252.

(5) Amine, K.; Belharouak, I.; Chen, Z.; Tran, T.; Yumoto, H.; Ota, N.; Myung, S. T.; Sun, Y. K. Nanostructured Anode Material for High-Power Battery System in Electric Vehicles. *Adv. Mater.* **2010**, *22*, 3052−3057.

(6) Mahmood, N.; Hou, Y. Electrode Nanostructures in Lithium-Based Batteries. *Adv. Sci.* **2014**, *1*, No. 1400012.

(7) Park, K. S.; Kang, J. G.; Choi, Y. J.; Lee, S.; Kim, D. W.; Park, J. G. Long-Term, High-Rate Lithium Storage Capabilities of TiO2 Nanostructured Electrodes Using 3D Self-Supported Indium Tin Oxide Conducting Nanowire Arrays. *Energy Environ. Sci.* **2011**, *4*, 1796−1801.

(8) Ren, Y.; Armstrong, A. R.; Jiao, F.; Bruce, P. G. Influence of Size on the Rate of Mesoporous Electrodes for Lithium Batteries. *J. Am. Chem. Soc.* **2010**, *132*, 996−1004.

DOI: 10.1021/acsomega.7b00289
ACS Omega 2017, 2, 1679−1686

(9) Saravanan, K.; Ananthanarayanan, K.; Balaya, P. Mesoporous TiO2 with High Packing Density for Superior Lithium Storage. *Energy Environ. Sci.* **2010**, *3*, 939.
(10) Hassoun, J.; Panero, S.; Simon, P.; Taberna, P. L.; Scrosati, B. High-Rate, Long-Life Ni-Sn Nanostructured Electrodes for Lithium-Ion Batteries. *Adv. Mater.* **2007**, *19*, 1632−1635.
(11) Lee, K.; Song, S. One-Step Hydrothermal Synthesis of Mesoporous Anatase TiO2 Microsphere and Interfacial Control for Enhanced Lithium Storage Performance. *ACS Appl. Mater. Interfaces* **2011**, 3697−3703.
(12) Qu, B.; Zhang, M.; Lei, D.; Zeng, Y.; Chen, Y.; Chen, L.; Li, Q.; Wang, Y.; Wang, T. Facile Solvothermal Synthesis of Mesoporous Cu(2)SnS(3) Spheres and Their Application in Lithium-Ion Batteries. *Nanoscale* **2011**, *3*, 3646−3651.
(13) Si, W.; Wu, X.; Zhou, J.; Guo, F.; Zhuo, S.; Cui, H.; Xing, W. Reduced Graphene Oxide Aerogel with High-Rate Supercapacitive Performance in Aqueous Electrolytes. *Nanoscale Res. Lett.* **2013**, *8*, No. 247.
(14) Worsley, M. A.; Pauzauskie, P. J.; Olson, T. Y.; Biener, J.; Satcher, J. H.; Baumann, T. F. Synthesis of Graphene Aerogel with High Electrical Conductivity. *J. Am. Chem. Soc.* **2010**, 14067−14069.
(15) Brun, N.; Sakaushi, K.; Yu, L.; Giebeler, L.; Eckert, J.; Titirici, M. M. Hydrothermal Carbon-Based Nanostructured Hollow Spheres as Electrode Materials for High-Power Lithium-Sulfur Batteries. *Phys. Chem. Chem. Phys.* **2013**, *15*, 6080−6087.
(16) Magasinski, A.; Dixon, P.; Hertzberg, B.; Kvit, A.; Ayala, J.; Yushin, G. High-Performance Lithium-Ion Anodes Using a Hierarchical Bottom-up Approach. *Nat. Mater.* **2010**, *9*, 353−358.
(17) Sun, B.; Chen, Z.; Kim, H. S.; Ahn, H.; Wang, G. MnO/C Core-Shell Nanorods as High Capacity Anode Materials for Lithium-Ion Batteries. *J. Power Sources* **2011**, *196*, 3346−3349.
(18) Xiao, Z.; Xia, Y.; Ren, Z.; Liu, Z.; Xu, G.; Chao, C.; Li, X.; Shen, G.; Han, G. Facile Synthesis of Single-Crystalline Mesoporous α-Fe2O3 and Fe3O4 Nanorods as Anode Materials for Lithium-Ion Batteries. *J. Mater. Chem.* **2012**, *22*, 20566.
(19) Wang, G.; Shen, X.; Yao, J.; Park, J. Graphene Nanosheets for Enhanced Lithium Storage in Lithium Ion Batteries. *Carbon* **2009**, *47*, 2049−2053.
(20) Kang, J. G.; Park, J. G.; Kim, D. W. Superior Rate Capabilities of SnS Nanosheet Electrodes for Li Ion Batteries. *Electrochem. commun.* **2010**, *12*, 307−310.
(21) Ji, L.; Yao, Y.; Toprakci, O.; Lin, Z.; Liang, Y.; Shi, Q.; Medford, A. J.; Millns, C. R.; Zhang, X. Fabrication of Carbon Nanofiber-Driven Electrodes from Electrospun Polyacrylonitrile/polypyrrole Bicomponents for High-Performance Rechargeable Lithium-Ion Batteries. *J. Power Sources* **2010**, *195*, 2050−2056.
(22) Sahay, R.; Suresh Kumar, P.; Aravindan, V.; Sundaramurthy, J.; Chui Ling, W.; Mhaisalkar, S. G.; Ramakrishna, S.; Madhavi, S. High Aspect Ratio Electrospun CuO Nanofibers as Anode Material for Lithium-Ion Batteries with Superior Cycleability. *J. Phys. Chem. C* **2012**, *116*, 18087−18092.
(23) Zhu, Y.; Han, X.; Xu, Y.; Liu, Y.; Zheng, S.; Xu, K.; Hu, L.; Wang, C. Electrospun Sb/C Fibers for a Stable and Fast Sodium-Ion Battery Anode. *ACS Nano* **2013**, *7*, 6378−6386.
(24) Vu, A.; Qian, Y.; Stein, A. Porous Electrode Materials for Lithium-Ion Batteries-How to Prepare Them and What Makes Them Special. *Adv. Energy Mater.* **2012**, *2*, 1056−1085.
(25) Wan, Y.; Shi, Y.; Zhao, D. Designed Synthesis of Mesoporous Solids via Nonionic-Surfactant-Templating Approach. *Chem. Commun.* **2007**, *9*, 897−926.
(26) Kim, H.; Cho, J. Superior Lithium Electroactive Mesoporous Si @ Carbon Core - Shell Nanowires for Lithium Battery Anode Material. *Nano Lett.* **2008**, *8*, 3688−3691.
(27) Cho, J. Porous Si Anode Materials for Lithium Rechargeable Batteries. *J. Mater. Chem.* **2010**, *20*, 4009.
(28) Das, S. K.; Darmakolla, S.; Bhattacharyya, A. J. High Lithium Storage in Micrometre Sized Mesoporous Spherical Self-Assembly of Anatase Titania Nanospheres and Carbon. *J. Mater. Chem.* **2010**, *20*, 1600.
(29) Shiva, K.; Asokan, S.; Bhattacharyya, A. J. Improved Lithium Cyclability and Storage in a Multi-Sized Pore ("differential Spacers") Mesoporous SnO2. *Nanoscale* **2011**, *3*, 1501−1503.
(30) Gasparotto, L. H. S.; Prowald, A.; Borisenko, N.; El Abedin, S. Z.; Garsuch, A.; Endres, F. Electrochemical Synthesis of Macroporous Aluminium Films and Their Behavior towards Lithium Deposition/stripping. *J. Power Sources* **2011**, *196*, 2879−2883.
(31) Ke, F.-S.; Huang, L.; Wei, H.-B.; Cai, J.-S.; Fan, X.-Y.; Yang, F.-Z.; Sun, S.-G. Fabrication and Properties of Macroporous Tin−cobalt Alloy Film Electrodes for Lithium-Ion Batteries. *J. Power Sources* **2007**, *170*, 450−455.
(32) Chao, D.; Xia, X.; Liu, J.; Fan, Z.; Ng, C. F.; Lin, J.; Zhang, H.; Shen, Z. X.; Fan, H. J. A V2O5/conductive-Polymer Core/shell Nanobelt Array on Three-Dimensional Graphite Foam: A High-Rate, Ultrastable, and Freestanding Cathode for Lithium-Ion Batteries. *Adv. Mater.* **2014**, *26*, 5794−5800.
(33) Huang, X.; Zeng, Z.; Fan, Z.; Liu, J.; Zhang, H. Graphene-Based Electrodes. *Adv. Mater.* **2012**, *24*, 5979−6004.
(34) Liu, S.; Yin, X.; Hao, Q.; Zhang, M.; Li, L.; Chen, L.; Li, Q.; Wang, Y.; Wang, T. Chemical Bath Deposition of SnS2 Nanowall Arrays with Improved Electrochemical Performance for Lithium Ion Battery. *Mater. Lett.* **2010**, *64*, 2350−2353.
(35) Pan, Q.; Wang, M.; Wang, Z. Facile Fabrication of Cu[sub 2]O/CuO Nanocomposite Films for Lithium-Ion Batteries via Chemical Bath Deposition. *Electrochem. Solid-State Lett.* **2009**, *12*, A50.
(36) Chou, S.-L.; Pan, Y.; Wang, J.; Liu, H.; Dou, S. Small Things Make a Big Difference: Binder Effects on the Performance of Li and Na Batteries. *Phys. Chem. Chem. Phys.* **2014**, *16*, 20347−20359.
(37) Liu, G.; Zheng, H.; Simens, A. S.; Minor, A. M.; Song, X.; Battaglia, V. S. Optimization of Acetylene Black Conductive Additive and PVDF Composition for High-Power Rechargeable Lithium-Ion Cells. *J. Electrochem. Soc.* **2007**, *154*, A1129.
(38) Qiu, L.; Shao, Z.; Wang, D.; Wang, W.; Wang, F.; Wang, J. Carboxymethyl Cellulose Lithium (CMC-Li) as a Novel Binder and Its Electrochemical Performance in Lithium-Ion Batteries. *Cellulose* **2014**, *21*, 2789−2796.
(39) Zhong, C.; Wang, J. Z.; Chou, S. L.; Konstantinov, K.; Rahman, M.; Liu, H. K. Nanocrystalline NiO Hollow Spheres in Conjunction with CMC for Lithium-Ion Batteries. *J. Appl. Electrochem.* **2010**, *40*, 1415−1419.
(40) Yue, L.; Zhang, L.; Zhong, H. Carboxymethyl Chitosan: A New Water Soluble Binder for Si Anode of Li-Ion Batteries. *J. Power Sources* **2014**, *247*, 327−331.
(41) Sun, M.; Zhong, H.; Jiao, S.; Shao, H.; Zhang, L. Investigation on Carboxymethyl Chitosan as New Water Soluble Binder for LiFePO4 Cathode in Li-Ion Batteries. *Electrochim. Acta* **2014**, *127*, 239−244.
(42) Han, Z.-J.; Yabuuchi, N.; Shimomura, K.; Murase, M.; Yui, H.; Komaba, S. High-Capacity Si−graphite Composite Electrodes with a Self-Formed Porous Structure by a Partially Neutralized Polyacrylate for Li-Ion Batteries. *Energy Environ. Sci.* **2012**, *5*, 9014.
(43) Zhang, Z.; Bao, W.; Lu, H.; Jia, M.; Xie, K.; Lai, Y.; Li, J. Water-Soluble Polyacrylic Acid as a Binder for Sulfur Cathode in Lithium-Sulfur Battery. *ECS Electrochem. Lett.* **2012**, *1*, A34−A37.
(44) Sun, J.; Huang, Y.; Wang, W.; Yu, Z.; Wang, A.; Yuan, K. Application of Gelatin as a Binder for the Sulfur Cathode in Lithium-Sulfur Batteries. *Electrochim. Acta* **2008**, *53*, 7084−7088.
(45) Wang, Q.; Wang, W.; Huang, Y.; Wang, F.; Zhang, H.; Yu, Z.; Wang, A.; Yuan, K. Improve Rate Capability of the Sulfur Cathode Using a Gelatin Binder. *J. Electrochem. Soc.* **2011**, *158*, A775.
(46) Shao, D.; Zhong, H.; Zhang, L. Water-Soluble Conductive Composite Binder Containing PEDOT: PSS as Conduction Promoting Agent for Si Anode of Lithium-Ion Batteries. *ChemElectroChem* **2014**, *1*, 1679−1687.
(47) Pan, J.; Xu, G.; Ding, B.; Chang, Z.; Wang, A.; Dou, H.; Zhang, X. PAA/PEDOT:PSS as a Multifunctional, Water-Soluble Binder to Improve the Capacity and Stability of Lithium-Sulfur Batteries. *RSC Adv.* **2016**, *6*, 40650−40655.

DOI: 10.1021/acsomega.7b00289
ACS Omega 2017, 2, 1679−1686

(48) Wang, Y.; Gozen, A.; Chen, L.; Zhong, W.-H. Gum-Like Nanocomposites as Conformable, Conductive, and Adhesive Electrode Matrix for Energy Storage Devices. *Adv. Energy Mater.* **2016**, No. 1601767.
(49) Li, W.; Zhang, Q.; Zheng, G.; Seh, Z. W.; Yao, H.; Cui, Y. Understanding the Role of Different Conductive Polymers in Improving the Nanostructured Sulfur Cathode Performance Understanding the Role of Different Conductive Polymers in Improving the Nanostructured Sulfur Cathode Performance. *Nano Lett.* **2013**, *13*, 5534−5540.
(50) Cui, Y.; Wen, Z.; Lu, Y.; Wu, M.; Liang, X.; Jin, J. Functional Binder for High-Performance LieO2 Batteries. *J. Power Sources* **2013**, *244*, 614−619.
(51) Zorbas, V.; Smith, A. L.; Xie, H.; Ortiz-acevedo, A.; Dalton, A. B.; Dieckmann, G. R.; Draper, R. K.; Baughman, R. H.; Musselman, I. H. Importance of Aromatic Content for Peptide/Single-Walled Carbon Nanotube Interactions. *J. Am. Chem. Soc.* **2005**, *127*, 12323−12328.
(52) Zorbas, V.; Ortiz-Acevedo, A.; Dalton, A. B.; Yoshida, M. M.; Dieckmann, G. R.; Draper, R. K.; Baughman, R. H.; Jose-Yacaman, M.; Musselman, I. H. Preparation and Characterization of Individual Peptide-Wrapped Single-Walled Carbon Nanotubes. *J. Am. Chem. Soc.* **2004**, *126*, 7222−7227.
(53) Liu, T.; et al. Facilitating Protein Denaturation in Organic Solvent and the Contribution to the Promoting Dispersion of Graphite Nanoplatelets in a Polymer. *Express Polym. Lett.* **2015**, *9*, 686−694.
(54) Fu, X.; Jewel, Y.; Wang, Y.; Liu, J.; Zhong, W. H. Decoupled Ion Transport in a Protein-Based Solid Ion Conductor. *J. Phys. Chem. Lett.* **2016**, *7*, 4304−4310.
(55) Ji, J.; Li, B.; Zhong, W. H. An Ultraelastic Poly(ethylene Oxide)/soy Protein Film with Fully Amorphous Structure. *Macromolecules* **2012**, *45*, 602−606.
(56) Jewel, Y.; Liu, T.; Eyler, A.; Zhong, W. H.; Liu, J. Potential Application and Molecular Mechanisms of Soy Protein on the Enhancement of Graphite Nanoplatelet Dispersion. *J. Phys. Chem. C* **2015**, *119*, 26760−26767.
(57) Souzandeh, H.; Johnson, K. S.; Wang, Y.; Bhamidipaty, K.; Zhong, W.-H. Soy-Protein-Based Nanofabrics for Highly Efficient and Multifunctional Air Filtration. *ACS Appl. Mater. Interfaces* **2016**, *8*, 20023−20031.
(58) Nikitin, M. P.; Zdobnova, T. A.; Lukash, S. V.; Stremovskiy, O. A.; Deyev, S. M. Protein-Assisted Self-Assembly of Multifunctional Nanoparticles. *Proc. Natl. Acad. Sci. U.S.A.* **2010**, *107*, 5827−5832.
(59) Luque, D.; Escosura, A. D. L.; Snijder, J.; Brasch, M.; Burnley, R. J.; Koay, M. S. T.; Carrascosa, J. L.; Wuite, G. J. L.; Roos, W. H.; Heck, A. J. R.; et al. Self-Assembly and Characterization of Small and Monodisperse Dye Nanospheres in a Protein Cage. *Chem. Sci.* **2014**, *5*, 575.
(60) Goriparti, S.; Harish, M. N. K.; Sampath, S. Ellagic Acid–a Novel Organic Electrode Material for High Capacity Lithium Ion Batteries. *Chem. Commun.* **2013**, *49*, 7234−7236.

DOI: 10.1021/acsomega.7b00289
ACS Omega 2017, 2, 1679−1686